Transport properties of CuPc based devices: a combined experimental and theoretical studies

C. Schuster[a], M. Kraus, A. Opitz[b], W. Brütting, U. Eckern

Institut für Physik, Universität Augsburg, 86135 Augsburg, Germany

Abstract. The electronic structure and the transport properties of copper phthalocyanine (CuPc), an organic semiconductor, attached to leads are investigated using density functional theory (DFT) the non-equilibriums Green's function formalism. Mainly, we discuss the electronic structure of CuPc attached to gold chains – a prototypical one-dimensional molecular device, which shall serve as model system for CuPc in transistors. We determine, in particular, the charge density of the HOMO (highest occupied molecular orbital) and LUMO (lowest unoccupied molecular orbital). For CuPc molecules attached to leads either the HOMO or LUMO is shifted to the Fermi level of the contact, thus electrons are transfered to the leads or onto the molecule, respectively, depending on the contact geometry. For a planar contact, the material and the dimensionality of the contacts does not influence the shape of the molecular orbitals. In all studied cases, electrons are injected onto the molecule. On the other hand, molecules contacted in perpendicular geometry, become hole doped. In addition, we determine the transmission coefficient and the I-V characteristic. By comparing density of states and transmission coefficient we can show which molecular levels can transmit charge. Thereby we see, that molecular orbitals localized on the Cu do not contribute to the transport in planar geometry, but provide the transmitting channel in perpendicular contact geometry. Finally we compare to contacts with two molecules in the contact region and fluorinated F_{16}CuPc.

1 Introduction

In the recent years the the theoretical description of experimental results became an imported issue for the understanding of the charge carrier transport in organic devices. The parameter-free calculation of the transport behaviour is realised only for single-molecule device. There the properties of the molecules and the contacts can be described by density functional theory (DFT) and the transport of charge carriers by _____. In contrast two-dimensional drift-diffusion simulation with commercial programs are used to model organic thin film devices [**?**]. Therefore exponential density of states are included into this software.

As a class of planar aromatic compounds, metal phthalocyanine (MPc) are considered for numerous applications since they show various physical and chemical properties. In particular, the semiconducting CuPc is applied in several optoelectronic devices [9]. It is used as buffer layer in organic light emitting diodes [10] or as active layer in organic field effect transistors [11]. Due to the narrow d-bands of the transition metal and the π-bonding present on the benzene rings CuPc crystals show effects related to electronic correlation. The correlation effects manifest for example in the Mott metal insulator transition upon K-doping [12,13]. Here, we are more interested in transport properties like charge injection and the mobility of the charge carriers as these are of practical interest for the use in optoelectronic devices.

[a] e-mail: Cosima.Schuster@physik.uni-augsburg.de
[b] e-mail: Andreas.Opitz@physik.uni-augsburg.de

In this paper we show a combined experimental and theoretical study. Whereas the experimental part were performed using field-effect devices for the theoretical part DFT calculations and non-equilibriums Green's function formalism were used. Both parts attend to the comparison of different contact geometries in the anisotropic CuPc system.

2 Materials and methods

Field-effect devices were fabricated on highly doped p^{++}-Si wafers with $320\,\mathrm{nm}$ thermally grown SiO_2 acting as gate electrode and gate dielectric, respectively. A schematic sketch of the OFETs can be seen in Fig. 1c. The wafers have been purchased from Si-Mat, Germany. Cleaning of the wafers was performed in an ultrasonic bath with acetone and isopropanol successively. After cleaning, on top of the SiO_2 surface PMMA was spin coated as passivation layers. PMMA was spin-coated from a $1.0\,\mathrm{wt.\%}$ solution in Toluene. CuPc has been purchased from Sigma Aldrich as sublimation grade and additionally purified by temperature gradient sublimation. CuPc was evaporated at a pressure of $1.0 \times 10^{-7}\,\mathrm{mbar}$ and a rate of $0.2\,\mathrm{\mathring{A}/s}$. The active semiconductor layer consists of a $25\,\mathrm{nm}$ thick layer of CuPc deposited on top of the passivated substrates for FET measurements and of a $50\,\mathrm{nm}$ thick layer for MIS diodes. For the transistors, top source and drain contacts were evaporated through a shadow mask with various channel lengths in the range of $30\,\mu\mathrm{m}$ to $350\,\mu\mathrm{m}$ using different metal contact with a thickness of $50\,\mathrm{nm}$. The thickness of the F_4TCNQ layer is about 1 nm.

The surface morphology of the CuPc layer was characterized by scanning force microscopy (SFM). SFM measurements were performed using a Thermo Microscopes Autoprobe CP-Research. Transistor characteristics were measured using a Keithley 4200 Semiconductor Parameter Analyzer and for the impedance spectroscopy a Solartron 1260 impedance/gain-phase analyzer coupled with a Solartron 1296 dielectric interface.

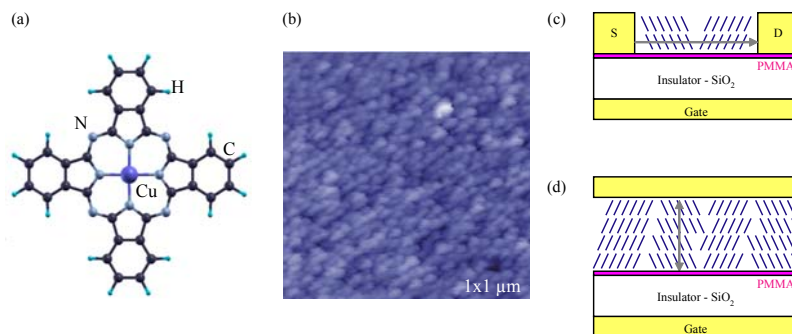– Device analysis (mobility determination, single curve and transfer length method)

Fig. 1. (a) Molecular structure of CuPc. (b) Scanning force microscopy image of an evaporated CuPc film deposited on PMMA passivation layer. The height scale is about 9 nm from black to white. (c) and (d) Schematic structure of the used field-effect devices – field-effect transistor and MIS diode, respectively. The gray arrows illustrate the charge transport direction in the devices. The molecules are standing on this substrate surface. The observed grain boundaries are also illustrated.

3 Ambipolar field-effect devices

The feature of ambipolar charge carrier transport in field-effect devices is related to the accumulation of both charge carrier types, electrons and holes, at the semiconductor/insulator interface. To prevent traps at the oxide surface an polymeric insulator is used in this study as passivation layer [2,14]. For both device types, FET and MIS diode, the accumulation is observed as shown in figure 2 and 3 by using gold electrodes. The accumulation of charge carriers depends on the applied gate voltage. Whereas electrons can be accumulated by applying a positive gate voltage, holes will be accumulated by applying a negative gate voltage. The accumulation of the respective charge carriers leads to a drain current in an FET and to a capacitance comparable to the insulator capacitance in an MIS diode. In dependence on the gate voltage the switch-on voltage (FET) or the flatband voltage (MIS diode) can be defined as voltage where the accumulation starts. Between the starting voltages for accumulation of holes and electrons the region of depletion is measured. There the current of an FET is in the noise level and the capacitance of the MIS diode is defined by a series circuit of the insulator and the semiconductor capacitance.

By variation the electrodes the transport switched to unipolar behaviour (see figure 2). Thereby the injection of one of the charge carrier types are pronounced and the other on is suppressed. By using Ca electrodes instead of Au the injection of electrons is enhanced by using a low work function electrode material and unipolar electron transport can be detected. In contrast by using a F_4TCNQ interlayer the injection of electrons can be suppressed and unipolar hole transport is observed. Using the TLM for determining the charge charier mobilities can be determined with consideration of the contact resistances as collected in table 1. This analysis shows that the mobilities are intrinsic material parameters and independent on the electrode materials [14]. For CuPc in this system the difference of the electron and hole mobilities is less than one order of magnitude with a higher hole mobility.

The transition from accumulation to depletion in the MIS diode can be seen in the capacitance spectroscopy using C-V and C-f measurements. The determined mobilities from the ambipolar MIS diode are also given in table 1 which is possible due to the wide depletion region [3]. The values of the mobilities are four to five orders of magnitude lower than the mobilities in the FETs. The difference of the electron and the hole mobilities is less pronounced.
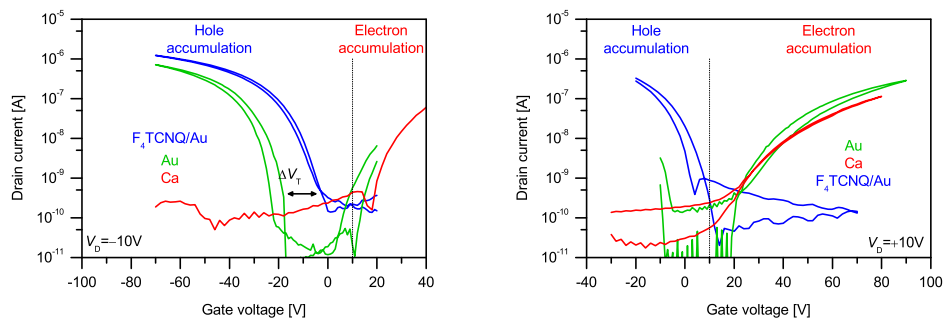

Fig. 2. Transfer characteristics of CuPc FETs in the top-contact configuration with different electrodes: calcium, gold and F_4TCNQ/gold.

Table 1. Room temperature mobilities for electrons and holes in FETs using different electrode materials and in MIS diodes suing gold contacts.

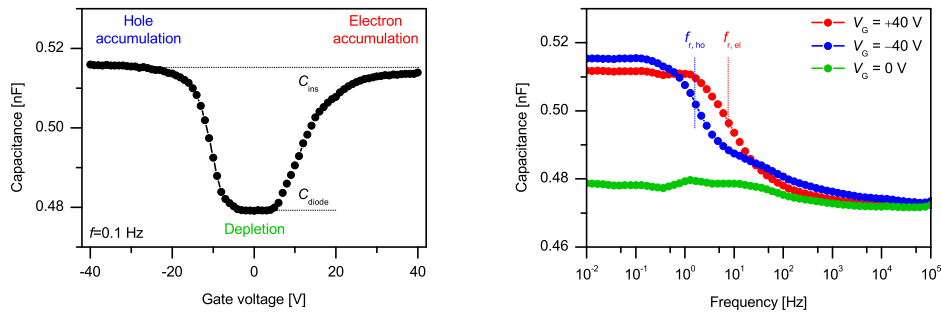| Devices	Electron transport	Hole transport
	Mobilities in FETs [cm^2/Vs]	
Ca contacts	3×10^{-4}	—
Au contacts	5×10^{-4}	2×10^{-3}
F_4CNQ/Au contacts	—	3×10^{-3}
	Mobilities in MIS diodes [cm^2/Vs]	
Au contacts	1×10^{-8}	3×10^{-8}

Fig. 3. Capacitance spectroscopy measurements (left: capacitance-voltage, right: capacitance-frequency) of CuPc MIS diode with gold top contacts.
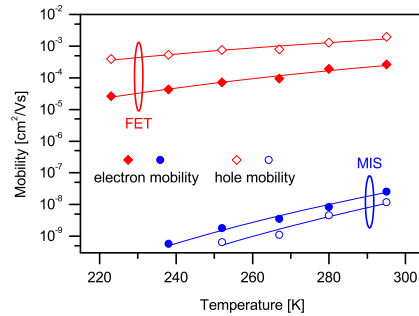

Fig. 4. Temperature dependent mobility for both field-effect transistor and MIS diodes as well as for both charge carrier types. The lines are fits to determine the activation energy using equation 1.

4 Charge carrier mobility

The temperature dependence of electron and hole mobilities for FET and MIS diode is shown in figure 4. The hole mobilities determined in an FET are for the whole temperature range higher than the electron mobilities and these both are higher than the mobilities determined in an MIS diode. Additionally the temperature dependence for the MIS diode mobilities are more pronounced than the temperature dependence of the FET mobilities. This difference of the mobilities between FET and MIS diode in terms of charge carrier density and anisotropy will be discussed in detail in the this section.

As a first step of analysis the activation energy of the temperature dependencies are given in table 2 which are determined by the following equation

$$\mu = \mu_0 \exp\left(-\frac{E_{\mathrm{act}}}{kT}\right). \tag{1}$$

Table 2. Activation energies for electrons and holes in ambipolar MIS diodes and ambipolar FETs determined by equation 1 as well as barrier energy in FETs determined by equation 2.

Devices	Electron transport	Hole transport
	Activation energy E_{act} [meV]	
MIS diode	410	452
Field-effect transistor	183	120
	Barrier energy E_{bar} [meV]	
Field-effect transistor	100	74

A strong difference of the activation energies is observed between the two device types and also between the two charge carrier types. Where as the hole mobility is higher and thereby the activation energy for holes is lower in the FET, the behaviour is reversed for the MIS diode. Additionally to the much lower mobilities in the MIS diode the activation energies for the MIS diodes are more than two times higher than the activation energies for the FET mobilities.

Whereas the transport in the FET is restricted to the accumulation layer with a high charge carrier density the transport in the MIS diode is enlarged over the whole device thickness. Thus the charge carrier density in the FET is determined by the effective gate voltage $(V_G - V_T)$ and in the range of $10^{19}\,\mathrm{cm}^{-3}$. In contrast the charge carrier density in the MIS diode in defined by the doping of the material which can be determined from the $C\text{-}V$ measurement. In the here analysed MIS diodes the charge carrier density is two orders of magnitude lower. To describe the dependence of the mobility on the charge carrier density extended disorder models were introduced. The extended Gaussian disorder model is applicable to polymeric systems [4,5], while the extended correlated disorder model can be used for molecular materials [6]. Both models are advantageous for disordered systems but not for (partially) ordered and anisotropic materials [7]. As the SFM image in figure 1b shows the CuPc film is polycrystalline. Therefore the description using a disorder parameter like the width of the Gaussian density of states is not applicable. For polycrystalline films the activation of hopping at the grain boundaries is the important parameter. The following temperature dependence [8]

$$\mu = \frac{qvl}{8kT} \exp\left(-\frac{E_{\mathrm{bar}}}{kT}\right) \qquad (2)$$

was given for thermionic emission of charge carriers at the grain boundaries. The barrier energy E_{bar} was determined for temperature dependence of the FET mobilities and is given in table 2. The barrier energies show the same tendency as the activation energies for the FET measurements. Related to the SFM image the grain boundary structure is only give in the plane parallel to the semiconductor/insulator interface this means for the transport in the FET accumulation layer. Perpendicular to this interface grain boundaries are absent.

Additionally to the ordered arrangement of the molecules the anisotropy needs to be considered. The CuPc molecules are standing on the surface as the schematic illustration of the devices in figure 1c shows. For this reason a good π-π overlap which supports the charge carrier transport in organic materials is present for the transport parallel to the semiconductor/insulator interface. Due to the standing molecules and the formation of π orbitals on the side of the disc-like molecule the overlap between CuPc molecules standing on top of each other is less pronounced. No models are available at the moment to uniformly describe the charge carrier density dependence and the anisotropic behaviour of the transport in organic films.

5 Computational details

In the following, we analyze the electronic structure, in particular the charge density of the HOMO (highest occupied molecular orbital) and LUMO (lowest unoccupied molecular orbital). In addition, we determine the transmission coefficient which is dominated by the HOMO and LUMO contributions. At last the corresponding IV characteristic is determined. In our calculations we use the DFT package SIESTA [15], which relies on a basis set of local atomic orbitals. In addition, SIESTA uses norm-conserving pseudo-potentials in the fully non-local form (Kleinman-Bylander [16]). For the metals Cu and Au, we apply pseudo-potentials including d valence states. Moreover, a double zeta basis set and the generalized gradient approximation for the exchange correlation potential are used. As CuPc contain a transition metal in an organic surrounding we have to ask for correlation effects and the best choice of the exchange correlation potential in our calculations. Spin polarization is necessary as the Cu^{2+} shows significant spin splitting [17]. In a systematic study, Marom et al. calculated the electronic structure of CuPc using local approximations as LDA and GGA and hybrid functionals as the semi-empirical B3LYP, the non-empirical PBE0 and the screened SHE03 [18]. The conclusion of their work concerning CuPc/metal systems is the advice to use the screened hybrid functional since it performs very well for CuPc and is not so bad for metals [19]. The B3LYP functional was used in a comprehensive study to detect and classify molecular orbitals of CuPc [20]. However, as we are interested in transport properties, the most important states near the Fermi level are sufficiently well described in GGA [18] and GGA is the best choice for noble metals [19], we decide to use GGA in the following. The overestimation of spin-splitting in the hybrids is a lack of these functionals. In some cases, a reduction of the exact exchange to values below 15% is necessary [21].

Several methods, based on electronic structure calculations, have been developed to address the problem of transmission through nano-contacts. In particular, two terminal contacts measurements are treated. Most computational methods rely on a combination of DFT and a scattering theory at the non-equilibrium Green's functions level, based on the Landauer–Büttiker scheme. The metallic leads are connected to a central region, in which the scattering takes place. In particular, our present study employs the SMEAGOL program package [22,23], a flexible and efficient implementation which consists of a direct summation of both open and closed scattering channels together with a regularization procedure for the Hamiltonian. As a consequence, materials with complex electronic structures can be tackled. In addition, spin polarized calculations are possible.

To apply the Landauer–Büttiker formalism, first the self-energies of the left (L) and right (R) lead are calculated. As metallic leads are used, the screening within the leads ensures that the distortion due to the contact/interface region decay within a few nanometer. Then the leads are connected to a central region of interest (molecule, nano-contact, interface), where the whole device is in equilibrium at the beginning. Thus, an effective description of the central region (C) is evaluated which includes the properties of the leads (L,R). In equilibrium, the transmission coefficient is given by the retarded Green's function G_M of the central (M) region and the lead self energies $\Sigma_{L/R}$, with $\Gamma_{L/R} := i[\Sigma_{L/R}(E) - \Sigma_{L/R}^\dagger(E)]$,

$$T(E, V = 0) = \text{Tr}[\Gamma_L G_C^\dagger \Gamma_R G_C]. \tag{3}$$

Then, the conductance is given by $G = \frac{2e^2}{h} T(E_F)$.

Applying an external voltage V, non-equilibrium Green's functions have to be considered; the charge density then can be calculated from the lesser Green's function

$$G_C^<(E) = iG_C(E)[\Gamma_L(E - eV/2) \cdot f(E + eV/2)$$
$$+ \Gamma_R(E + eV/2) \cdot f(E - eV/2)]G_C^\dagger(E), \tag{4}$$

with the Fermi function f. The current then can be written as

$$I(V) = \frac{e}{h} \int dE\, T(E, V)[f(E + eV/2) - f(E - eV/2)]. \tag{5}$$

6 Characteristics of the pristine CuPc molecule

Copper phthalocyanine is a flat molecule with fourfold rotation symmetry. The transition metal is surrounded by porphyrin and benzene rings, as indicated in Fig. 1.
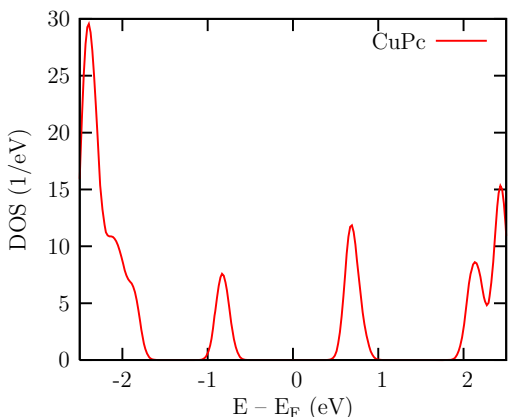
Fig. 5. Density of states for CuPc in the spinpolarized GGA calculation.

More or less identical photoemission spectra of CuPc thin films [20] and gase phase CuPc [24] suggest that electronic structure is hardly modified by inter-molecular interactions. Also the transport properties are considered to be intrinsic properties of the CuPc molecules. Therefore we can extract the transport properties of bulk systems from the calculation of single molecules. Before turning to the molecules in a contact, we summarize the results obtained for CuPc monolayers. CuPc molecules adsorbed on surfaces (metallic as well as insulating) form periodic monolayers. The typical molecule-molecule distances in a CuPc monolayer on top of an [111] directed surface of Au [25] or [110] surface of Ag [26] are longer than the molecule-molecule distances in the CuPc crystal [27]. The CuPc molecules in the monolayer show different orientation towards each other given by the symmetry of the substrate. Due to the long molecule-molecule distances within the monolayer, the electronic structure of the monolayer near the Fermi level is mainly the electronic structure of a single molecule with only minor effects of the coordination to the other molecules. We have checked this for a orientation of the molecules to each other of 60° and a molecule-molecule distance of d=14.4 Å (as obtained for a Au[111] substrate), a 90° orientation and d=17.35 Å (Ag[110] substrate), and 45° and d=17.35 Å as well as d=13.72 Å, where the last distance is the intermolecular distance within a CuPc crystal. In these calculations we only calculate the monolayer without the substrate. The density of states (DOS) near the Fermi level, shown in Fig. 5, where we used a level broadening of 0.1 eV to plot the DOS, is identical in all substrate configurations. In addition, it is in accordance with recent theoretical and experimental results [17,28]. Using the bulk distance, the gap is smaller than in the monolayer, in accordance with previous results [20]. The band gap of the substrate configurations amounts to $\Delta \approx 1.65 eV$. In particular, the HOMO includes contribution of the $b_{1g\uparrow}$ orbital localized on the Cu together with the a_{1u} molecular orbital and the LUMO the $b_{1g\downarrow}$ together with the molecular e_g. The charge density isosurface plot of the states contributing to the HOMO and LUMO is shown in Fig. 6. As compared to [20], the LUMO has the same shape within GGA and B3LYP. In case of the HOMO, the Cu b_{1g} contributes in GGA but not in B3LYP. The most important difference of the HOMO versus LUMO lies in the missing contribution on the nitrogen in the HOMO. Otherwise the spatial extension is similar. Additional charges on the molecules do not change the shapes of the molecular orbitals. In our calculations we have charged the unit cell – containing one molecule – with an extra electron or removed one electron. Concerning the structure we find slight deviations from the planar behavior but the curvature is very small. When adding or removing electrons the HOMO/LUMO peak in the DOS is shifted to the Fermi level as expected. Drawing the charge density isosurface of the states contributing to the peak at the Fermi level, we see that the charging of the molecule does not alter the shape of the molecular orbitals. In other words, the electronic structure does not change by doping.

7 CuPc with contacts

As discussed above, it is suggested that the transport properties seen in experiments are determined by the transport properties of the individual molecules. For this reason we consider in the following single
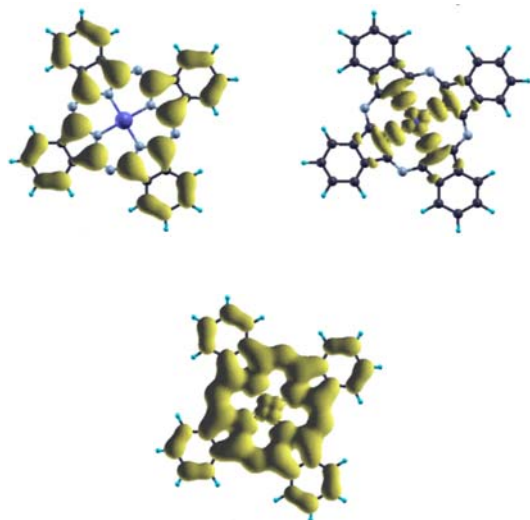
Fig. 6. Upper row: the HOMO contains contribution of the a_{1u} orbital (left hand side) and of the b_{1g} orbital (right hand side) located on the copper. Lower row: the LUMO, contains contribution of the e_g orbital and of the b_{1g} orbital. Here, the sum of both contributions is plotted.
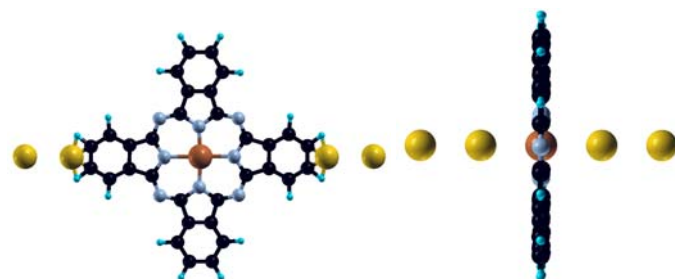

Fig. 7. Top: On top view on the planar contact. The distance between Au-H and Au-C is given by $d_{\mathrm{Au-H/C}}$=1.37 Å. Bottom: Sideview on the perpendicular contact. The distance between Au-Cu is given by $d_{\mathrm{Cu-Au}}$=2.89 Å.

CuPc molecules contacted to leads in two different contact geometries. In the first configuration the the contact of the leads to the molecule is established via the outer H-C-H atoms in a planar transport geometry. Experimentally, this configuration – a prototypical one-dimensional system – was realized by placing the CuPc molecule and Au atom with an STM tip on a NiAl substrate [29]. The structure is shown in Fig. 7. The distance between Au-H, $d_{\mathrm{Au-H}}$=1.37 Å, and Au-C $d_{\mathrm{Au-C}}$=1.37 Å, which we use in the calculations is obtained by molecular dynamics. Using the planar we compare contacts made of different materials – Au chains versus bulk Ca contacts – to determine the influence of the material and dimensionality of the leads. As other materials like Ca do not form chains we contact the CuPc molecule to bulk Ca in [001] FCC direction using a pyramidal contact geometry.

For the second configuration we use again Au chains as leads but investigate a perpendicular contact geometry. In the second case, we contact directly to the Cu, simulating a transverse transport measurement. Here, the distance between Au-Cu, $d_{\mathrm{Cu-Au}}$=2.89 Å, is chosen as the distance within the Au chains, with no resulting forces. A sideview on the perpendicular structure is shown in Fig. 7.

Concerning the electronic structure of the planar contact, the DOS projected on the CuPc states shows contributions at the Fermi level, see Fig. 8, in case of Au and Ca contacts. In addition, the charge density isosurface of the states between -0.3 and 0.7 eV in case of Au contacts and the charge density isosurface of the states between -0.3 and 0.4 eV in case of Ca contact is more or less identical, see Fig. 9. For this reason, we expect similar transport properties of Au and Ca contacted molecules. Moreover, the shape of the molecular orbital near E_F resembles the LUMO of the free molecule, indicating an electron transfer to the molecule due to the contacts. As the shape of the molecular orbitals does not
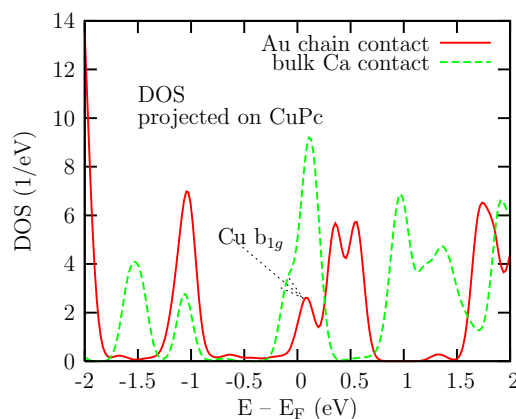
Fig. 8. DOS for CuPc contacted to Au chains or Ca bulk leads.
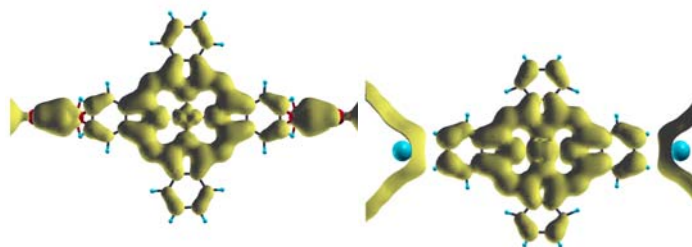

Fig. 9. Top: charge density isosurface plot of the LDOS at the Fermi level for CuPc contacted to Au chains. Bottom: charge density isosurface plot of the LDOS at the Fermi level for CuPc contacted to bulk Ca. In both cases, electrons are injected into the molecule.

change due to the contact to the leads, the transport properties are determined by the properties of the isolated molecule. However, in case of the Au chain contacts, the Cu shows a finite magnetic moment, whereas the Cu moment is zero in case of the Ca leads. Analyzing the contributions at the Fermi energy of the Au contacted molecule in detail, we see that the Cu b_{1g} dominates between -0.3 and 0.3 eV, whereas the e_g dominates around 0.5 eV. An overlap of the electronic states of the leads and of the molecule is not present at E_F.

As far as the planar geometry is concerned, we observe only electron injection onto the molecule. We need another configuration to treat the hole injection. Testing Pt electrodes – Pt has the largest work function among the metals used as contacts – we find no overlap of the contact states with the molecular states, hence no contributions at the Fermi level, hence an insulating system. Injection of holes, i.e. a charge density isosurface near the Fermi level resembling the HOMO, on the other hand is found when considering a perpendicular contact, see Fig. 10.

Having analyzed the electronic structure, we turn now to the transport properties. Concerning the planar contact geometry, the transmission coefficient shows no resonance at the Fermi level as compared to the DOS projected on the CuPc states, see Fig. 11, top panel. To compare DOS and $T(E)$ we multiplied the DOS by 1/10. As the states at the Fermi level do not contribute to the transmission, the device operates in the tunneling regime. At the resonant molecular energy levels, given by the a_{1u} and e_g molecular orbitals, the transmission coefficient tends to one.

The off-resonance transmission coefficient of the perpendicular contact geometry is clearly higher, see Fig. 11, middle panel. The higher transmission traces back to the behavior of the DOS. The DOS of CuPc is rather high in the perpendicular contact with broad molecular levels nearby in energy as compared to the planar contact. The broadening of the molecular levels traces back to the short distance of the Au atoms at the left and right end of the leads in the perpendicular geometry. The states according
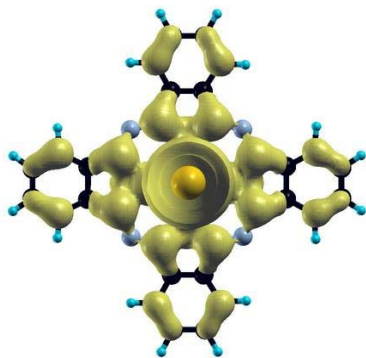
Fig. 10. Charge density isosurface plot of the LDOS at the Fermi level for CuPc contacted to Au chains in a perpendicular geometry.

to the molecular a_{1u} and e_g orbitals are found at -0.2 eV and 0.2 eV, respectively. Thus, the energy difference between the levels is smaller than in the planar configuration, where we find a level spacing of almost 1 eV. The a_{2u} orbital, i. e. the HOMO-1 of the free molecule, is found at -0.5 eV. Concerning the a_{2u} and e_g orbitals, the transport channels are given an Au-N-Au bridge.

The according IV characteristics of the planar and perpendicular contact are shown in Fig. 11, bottom. In case of the planar contact, we find a linear IV characteristic for non resonant transmission at low voltage, where the slope corresponds to $G \propto T(E_F)$. As the voltage increases, the transmission becomes resonant, and the I-V dependence non-linear, $I \propto V^{3/2}$. The IV characteristic of the perpendicular contact is given by $I \propto V^{1.28}$, up to V≈ 1V. The exponent is somehow an average of the non-resonant and resonant regime.

To summarize, we have shown that electrons are injected in a planar contact, independent of the material of the leads, whereas holes are injected in the perpendicular contact. Due to a smaller level spacing in the perpendicular contact, the transmission is about three orders of magnitude larger in the perpendicular contact.

8 Two molecules within the contact

As the transport in the diodes does not only depend on the injection at the contact, so to speak of the contact-molecule interaction, but also on the transport from molecule to molecule, we take into account the molecule molecule interaction by studying two molecules in the contact.

To obtain al crystal like arrangement we contact differently in the planar regime. Now we place the Au of the Au chain near the N atom between the benzene rings, as indicated in Fig. 12. In case of a single molecule this contact is not the lowest in energy, but possible [29]. In the perpendicular geometry we can easily stagger the molecules in row. The structures are shown in Fig. 12

The electron structure of the planar contact with two molecules show minor changes in comparison to the planar contact with one molecule, see Fig. 13, upper plot. The molecular a_{1u} orbital is found at -1 eV in both cases. The contribution of the e_g orbital, however is spread from -0.3 eV to 0.5 eV, similar to the Ca contact. These states at the Fermi level lead to a charge density isosurface with the shape of the CuPc LUMO. The splitted b_{1g} orbitals are found at -0.5 eV and 1 eV. The DOS of two CuPc attached to Au chain in perpendicular geometry, see Fig. 13 lower plot, shows distinct energy levels as compared to a single molecule in the contact. The smaller peaks at $\pm$ 0.6 eV are the contributions of the spin-split Cu b_{1g} orbitals. The higher peaks can be traced back to the a_{1u} and e_g molecular orbitals. In particular, the charge density isosurface of the states at E_F are similar to the HOMO on the molecule, i.e. without states at the Cu. The e_g is here the LUMO+1. The side peaks to the central peak at E_F are therefore given by the b_{1g} states of the Cu which give the transport path. The transport through the a_{1u} and e_g states is expected to be suppressed.
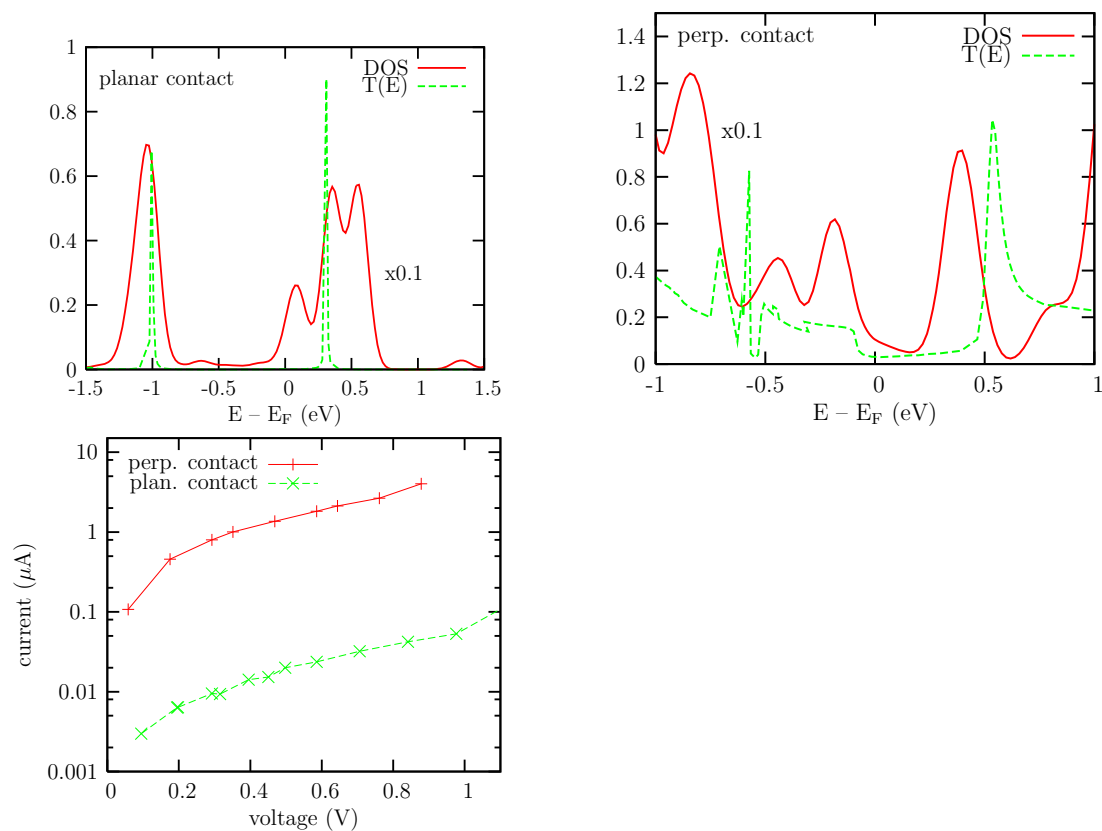
Fig. 11. Top: DOS projected on CuPc and T(E) of one CuPc molecule in planar contact geometry. Middle: DOS projected on CuPc and T(E) of one CuPc molecule in perpendicular contact geometry. Bottom: IV characteristic of the planar and perpendicular contact.
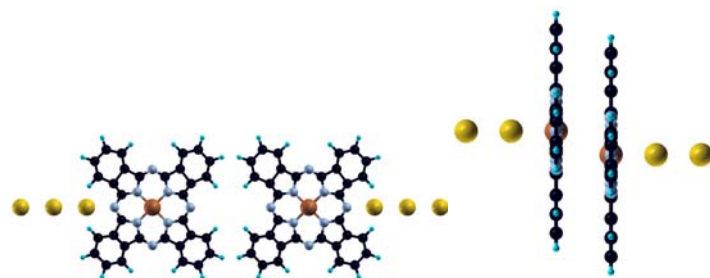

Fig. 12. Top: On top view of the planar contact with two molecules in the scattering region. Bottom: Sideview on the perpendicular contact. The Cu-Cu distances d=13.72 Å(planar) and d=3.79 Å(perpendicular), respectively, are chosen similar to the distances within the crystal.

In the perpendicular geometry with two CuPc molecules, the IV characteristic is linear up to 0.6 V. Then it changes to a steep increase with $I \propto V^{5/2}$. The increase coincide with the transport through the resonant molecular level at about 0.6 eV.

9 Summary

In summary we have analyzed the electronic structure of CuPc molecules attached to metallic leads in the ground state. As far as electrons are injected by the leads, which can be realized as well with Au chains or bulk Ca leads in the planar geometry, the shape of the charge density at the Fermi level
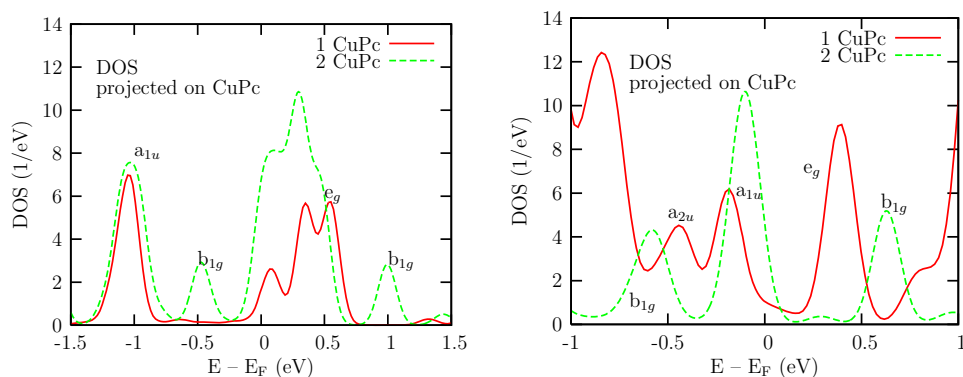
Fig. 13. DOS projected on CuPc, we compare one or two CuPc molecules between Au chains in the planar configuration (top) or in the perpendicular configuration (bottom).
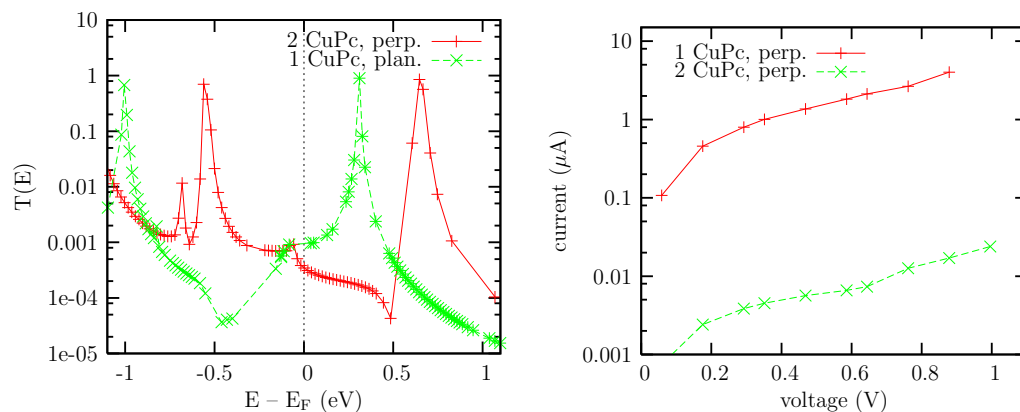

Fig. 14. Top: T(E) planar, still missing Bottom: Current through one and two molecules in the perpendicular configuration.

corresponds to the LUMO of an isolated molecule, hence electron transport with similar properties is expected. The perpendicular contact behaves differently. The states at the Fermi level resembles the HOMO of the isolated molecule, which can be interpreted as electron transfer to the leads. The density of states of the contacted molecule determines the transmission through the molecular contact. States which no spatial overlap of molecule and leads block the transmission. For this reason, even if states found at the at the Fermi level, the contacts can be nearly insulating.

10 Outlook: Predictions for fluorinated CuPc

As a material with different properties we have also calculated fluorinated CuPc. When analyzing the data for the $F_{16}CuPc$, see Fig. 15, the DOS of a monolayer shows the b_{1g} contribution at lower energies than the a_{1u} as compared to CuPc. When contacted to Au chains in the planar geometry, states at the Fermi level are induced, however the peak structure is different. We find a symmetric peak at E_F. As the peak structure of the perpendicular contact is more clear, we show only the DOS of two $F_{16}CuPc$ molecules within the perpendicular contact, see Fig. 15, lower plot. As compared to CuPc, the a_{1u} orbital is shifted to the Fermi level and the current is carried by the b_{1g} orbital at 0.5 eV. Concerning the charge density isosurface corresponding to the states at E_F, the charge density isosurface of the planar contact is not spread over the whole molecule as in case of CuPc but quenched towards the transport axis, see Fig. 16. The charge density isosurface corresponding to the states at E_F of the perpendicular contact, on the other hand, is found to be the same as in CuPc.
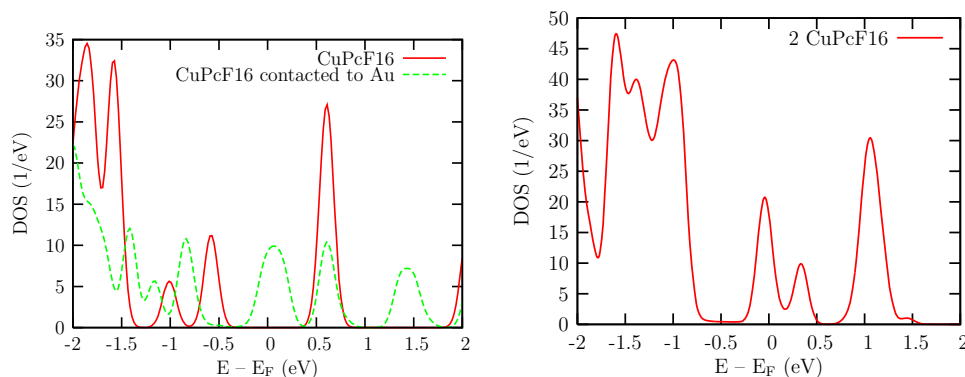
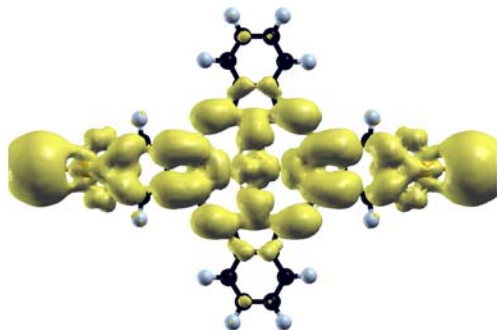**Fig. 15.** DOS $F_{16}CuPc$ contacted to Au chains in perpendicular (top) and planar (bottom) configuration.

Fig. 16. Charge density isosurface plot of the states at E_F for $F_{16}CuPc$ contacted to Au chains.

The transmission through $F_{16}CuPc$ in the planar contact is expected to be higher than through CuPc, since the DOS shows states at the Fermi level and the according charge density reveals an overlap of leads and molecular states. However, we find a steep increase of the current with voltage due to the resonance at E_F, but an decreasing current with increasing voltage in the non-resonant regime. Due to the sharpness of the transmission the current is suppressed for applied voltage and the current is almost two orders of magnitude smaller in case of $F_{16}CuPc$.

In the perpendicular configuration, the b_{1g} levels are the transport channels. As they do not differ between $F_{16}CuPc$ and CuPc, the current is almost the same.

Acknowledgements

References

1. S. Luan and G. W. Neudeck, J. Appl. Phys. **72** (1992) 766–772.
2. L. L. Chua, J. Zaumseil, J. F. Chang, E. C. W. Ou, P. K. H. Ho, H. Sirringhaus, and R. H. Friend, Nature **434** (2005) 194–199.
3. E. C. P. Smits, T. D. Anthopoulos, S. Setayesh, E. van Veenendaal, R. Coehoorn, P. W. M. Blom, B. de Boer, and D. M. de Leeuw, Phys. Rev. B **73** (2006) 205316.
4. R. Coehoorn, W. F. Pasveer, P. A. Bobbert, and M. A. J. Michels, Phys. Rev. B **72** (2005) 155206.

5. W. F. Pasveer, J. Cottaar, C. Tanase, R. Coehoorn, P. A. Bobbert, P. W. M. Blom, D. M. de Leeuw, and M. A. J. Michels, Phys. Rev. Lett. **94** (2005) 206601.

6. M. Bouhassoune, S. L. M. van Mensfoort, P. A. Bobbert, R. Coehoorn, Org. Electron. **10** (2009) 437–445.

7. S. Grecu, M. Roggenbuck, A. Opitz, and W. Brtting, Org. Electron. **7** (2006) 276-286.

8. R. Bourguiga, M. Mahdouani, S. Mansouri, and G. Horowitz, Eur. Phys. J. Appl. Phys. **39** (2007) 7-16.

9. Y Shirota and H Kageyama Chem. Rev. **107**, 953 (2007)

10. S. M. Tadayyon, H. M. Grandin, K. Griffiths, P. R. Norton, H. Aziz, and Z. D. Popovic, Organic Electronics **5**, 157 (2004)

11. M. Minagawa, K. Shinbo, K. Usuda, T. Takahashi, M. Iwasaki, K. Kato, and F. Kaneko Jpn. J. Appl. Phys. **45** 8890 (2006)

12. M. F. Craciun, S. Rogge and A. F. Morpurgo J. Am. Chem. Soc., **127**, 12210 (2005); M. F. Craciun, S. Rogge, M. J. L. den Boer, S. Margadonna, K. Prassides, Y. Iwasa, and A. F. Morpurgo, Advanced Materials **18**, 320 (2006)

13. G. Giovannetti, G. Brocks, J. van den Brink, Phys. Rev. B. **77**, 035133 (2008).

14. A. Opitz et al., NJP 10, 065006 (2008)

15. J. M. Soler, E. Artacho, J. D. Gale, A. García, J. Junquera, P. Ordejón, and D. Sánchez-Portal, J. Phys.: Condens. Matter **14**, 2745 (2002).

16. L. Kleinman and D. M. Bylander, Phys. Rev. Lett. **48**, 1425 (1982).

17. B. Bialek, I. G. Kim, and J. I. Lee, Thin Solid Films **436**, 107 (2003).

18. N. Marom, O. Hod, G. E. Scuseria, and L. Kronik, J. Chem. Phys. **128**, 164107 (2008).

19. J. Paier, M. Marsman, and G. Kresse, J. Chem. Phys. **127**, 024103 (2007).

20. V. Yu. Aristov, O. V. Molodtsova, V. V. Maslyuk, D. V. Vyalikh, V. M. Zhilin, Yu. A. Ossipyan, T. Bredow, I. Mertig, and M. Knupfer, Appl. Surf. Sci. **254**, 20 (2007); O. V. Molodtsova, M. Knupfer, V. V. Maslyuk, D.V̈. Vyalikh, V. M. Zhilin, Y. A. Ossipyan, T. Bredow, I. Mertig, and V. Yu. Aristov, J. Chem. Phys. **129**, 154705 (2008); V. Yu. Aristov, O. V. Molodtsova, V. V. Maslyuk, D. V. Vyalikh, V. M. Zhilin, Yu. A. Ossipyan, T. Bredow, I. Mertig, and M. Knupfer, J. Chem. Phys. **128**, 34703 (2008).

21. P. E. M. Siegbahn, J. Biol. Inorg. Chem. **11**, 695 (2006).

22. A. R. Rocha, V. M. Garcia-Suarez, S. W. Bailey, C. J. Lambert, J. Ferrer, and S. Sanvito, Nature Materials **4**, 335 (2005).

23. A. R. Rocha, V. M. Garcia-Suarez, S. W. Bailey, C. J. Lambert, J. Ferrer, and S. Sanvito, Phys. Rev. B **73**, 085414 (2006).

24. J. Berkovitz, J. Chem. Phys. **70**, 2819 (1979).

25. T. Fritz, M. Hara, W. Knoll, and H. Sasabe, Mol. Cryst. Liq. Cryst. **253**, 269 (1994)

26. F. Song, H. Huang, W. Dou. H. Zhang, Y. Hu, H. Qian, H. Li, P. He, S. Bao, Q. Chen, and W. Zhou, J. Phys.: Condens. Matter **19**, 136002 (2007).

27. C. J. Brown, J. Chem. Soc. (A), 2488 (1968).

28. S. F. Alvarado, L. Rossi, P. Mller and W. Rieß, Synthetic Metals **122**, 73 (2001).

29. G. V. Nazin, Qiu, and W. Ho, Science **302**, 77 (2003).